1. Introduction

The corona of the Sun is a million times fainter than the solar surface beneath, yet it is one of the most closely monitored objects in astronomy today. In 1943, Bengt Edlén (1943) showed conclusively that, contrary to physical expectations, the corona emitted spectral lines from ions with ten or more electrons removed, requiring particle temperatures some 2000 times that of the visible surface. The corona gained political importance during World War II because it radiates strong and variable extreme ultraviolet (EUV) and X-radiation, causing troublesome variations of the ionosphere that affected communications. The prediction and discovery of the solar wind originating from the corona late in the 1950s, and the first definitive observations of Coronal Mass Ejections (CMEs) in the early 1970s, further focused attention on the corona during the Cold War. SKYLAB identified the Sun's enigmatic magnetic fields as the driver of coronal physics and its effects on Earth. Today, a modest fleet of spacecraft and ground-based telescopes continuously monitors the Sun's surface magnetism, atmosphere and corona to avoid damage to electrical infrastructure upon which modern society is dependent.

While many observatories are devoted to operations with standard instruments, there remain mysteries at the heart of the corona. Just how the Sun generates, stores, transports and releases magnetic free energy to send high energy photons, particles and magnetic bubbles into space is a question still challenging our basic understanding of why the Sun (and all rotating stars with convection zones) must exhibit these phenomena. One purpose of the present proposed work is to explore critical aspects of energy propagation and dissipation within the corona exploiting the *infrared (IR) coronal spectrum*. Surprisingly, no survey has been made of the IR coronal spectrum, dominated by a continuum of light scattered by electrons and dust and punctuated by more intense spectral lines from cool prominence material as well as the hotter plasma. Another goal is therefore to acquire resolved and calibrated profiles of IR lines over a broad wavelength range from a high-altitude aircraft during total eclipse.

During the 8 April 2024 North American eclipse, a Michelson interferometer coupled with a two-dimensional (2D) IR detector will obtain high quality coronal data over the entire 1–4 μm spectral range for the first time. The Airborne Coronal Emission Surveyor (ACES) will observe from an altitude of about 14 km with a spectral resolution of 0.5 cm^{-1} and a spatial plate scale of $20''$ across a field of view of $2000'' \times 100''$ (2 $R_\odot \times$ 0.1 $R_\odot$). During its six-minute commissioning observation from the NSF/NCAR Gulfstream V High-performance Instrumented Airborne Platform for Environmental Research (GV HIAPER), ACES will seek more than twenty forbidden lines of ionized magnesium, aluminum, silicon, sulfur, argon, calcium, iron, and nickel, at least half of which have never been observed.

The IR has many advantages over the radio, EUV, and X-ray energies that form the vast bulk of modern monitoring and research. We have exploited some of these advantages in our earlier achievements documented below. Our novel research goals include: identifying the brightest spectral lines; documenting their widths and higher order properties of the line profiles; measuring contributions from collisional versus radiative excitation (scattering); documenting the variations of all of the above as a function of the features observed (e.g., streamer vs normal corona) and projected radius. Our analysis will seek to build upon earlier work at visible and ultraviolet (UV) wavelengths, in deriving electron temperatures, densities, ion temperatures, relative ion abundances, and inhomogeneous plasma densities from line and continuum coronal intensities, all using established techniques (e.g. line and continuum ratios, line profiles), extending measurements as far as possible from Sun center. The scattering contributions enable measurements of coronal lines at larger radii than EUV lines as well as also the generation of linear polarization with diagnostic potential for measuring magnetic connectivity within the corona. We will seek collaborations with researchers using space- and ground-based assets over the period of the proposed eclipse experiment, and with modelers to understand in particular earlier tentative relationships between electron and ion temperatures, extended

out to 2 $R_\odot$ from Sun center. Our data will be made freely available after full calibration, and the instrument will be curated at NCAR for use by the community.

2. Results from Prior NSF Support

The PI, Jenna Samra, and one Co-PI, Chad Madsen, were supported on the four projects below as either PI, Co-PI, or graduate student. Co-PI Paul Bryans has not had NSF support in the last five years.

2.1. MRI: Development of an Airborne Infrared Spectrometer (AIR-Spec) for Coronal Emission Line Observation

PI: Edward DeLuca, Co-PI: Leon Golub
Award #1531549, Amount: $1,200,591.00, Period of support: August 15, 2015–July 31, 2018

Intellectual Merit: During the 2017 total solar eclipse, AIR-Spec took a step toward the direct observation of coronal magnetic fields by measuring infrared emission in the solar corona from aboard GV HIAPER (Samra et al. 2022b). The instrument successfully observed its five target lines, Si X 1.43 µm, S XI 1.92 µm, Fe IX 2.85 µm, Mg VIII 3.03 µm, and Si IX 3.93 µm, which were identified by Judge (1998) as promising candidates for future spectropolarimetric observations based on abundance, charge state, branching ratios and collision destruction probabilities. During the eclipse observation, AIR-Spec measured the peak intensities, and center wavelengths of all five lines radially outward from the limb at four positions in the corona. The observation of Fe IX at 2.85 µm was the first of that line (Samra et al. 2018).

AIR-Spec was designed as a cryogenic slit spectrometer that measured light over a 1.55 $R_\odot$ field of view (FOV) in four spectral passbands between 1.4 and 4 µm (Samra et al. 2022b). The original package included an image stabilization system (the first to fly on the GV), feed telescope, grating spectrometer housed in a cryogenic vacuum chamber, and slit-jaw imager. The instrument development encountered a number of engineering challenges, centered around maintaining adequate resolution and signal-to-noise ratio (SNR) in a compact and inexpensive package on a moving platform, all of which were met to enable mission success.

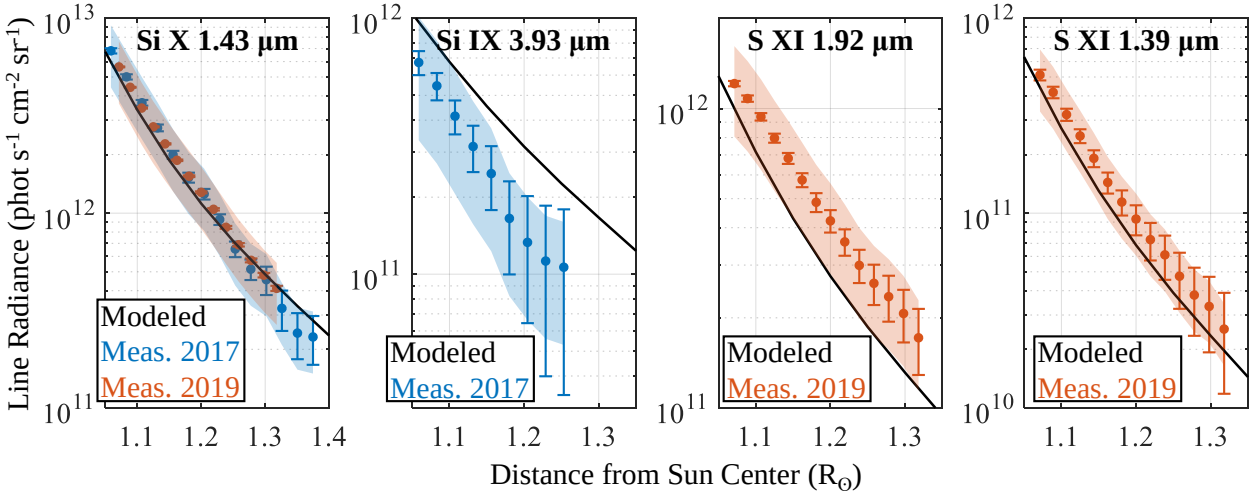

Figure 1. Line radiance vs. height. The error bars indicate 95% confidence intervals in the line fits. The shaded region spans two different radiometric calibrations, giving a measure of the calibration uncertainty.

The AIR-Spec measurements validated models by Del Zanna and DeLuca (2018) for the intensity of Si X and Si IX as a function of distance from the limb (Figure 1, left two panels). Coordinated observations between AIR-Spec and the Hinode Extreme Ultraviolet Spectrometer (EIS) were used to characterize the

coronal plasma near the west limb (Madsen et al. 2019). Our emission measure (EM) loci analysis ratioed observed AIR-Spec line intensities to modeled volume emissivities to predict a temperature between $10^{6.0}$ and $10^{6.2}$ K, similar to the temperature found with EIS.

Broader Impacts: The 2017 AIR-Spec mission provided training for students and early-career researchers and a unique opportunity for public outreach before and after the eclipse. The AIR-Spec instrument scientist, Jenna Samra, was a Harvard PhD student who wrote her thesis on the instrument design and development, the data processing and calibration, and the first science results from the 2017 eclipse observation. The project allowed Vanessa Marquez, a mid-career engineer at SAO, to develop her mechanical and optical engineering skills as she took the lead role in the instrument's mechanical design. Additionally, the project supported the training of a new postdoctoral fellow at SAO, Chad Madsen, who is now a full-time member of SAO's research staff and a Co-PI on this proposal. In 2016 and 2017, the AIR-Spec team mentored three students in SAO's Research Experience for Undergraduates (REU) program. All three students presented their work at meetings of the American Geophysical Union (AGU, Cervantes Alcala et al. 2016; Vira 2017), the American Astronomical Society (AAS, Fedeler et al. 2017), and/or the International Society for Optics and Photonics (SPIE, Vira et al. 2018).

The 2017 eclipse mission was covered by the press and provided many opportunities for outreach. The project and team were featured in articles in *The New York Times*, *The Washington Post*, *Nature*, *Smithsonian Air & Space Magazine*, *Science News*, and *Forbes*. Outreach presentations were given to high school students at the Montrose School (Medfield, MA) and Blair Academy (Blairstown, NJ), undergraduates at Smith College, and the public at a meeting of the New England Section of the Optical Society of America.

Publications: The 2017 project featured in four journal articles (Samra et al. 2018; Madsen et al. 2019; Judge et al. 2019; Samra et al. 2022b) and two conference papers (Samra et al. 2016; Vira et al. 2018).

2.2. Airborne InfraRed Spectrograph (AIR-Spec) 2019 Eclipse Flight

PI: Edward DeLuca, Co-PIs: Peter Cheimets, Jenna Samra, and Vanessa Marquez
Award #1822314, Amount: $519,286.00, Period of support: May 15, 2018–April 30, 2021

Intellectual Merit: The second AIR-Spec research flight took place during the July 2, 2019 total solar eclipse over the south Pacific (Samra et al. 2022a). Totality lasted for 9 minutes and produced 7 minutes of data in 9 slit positions. AIR-Spec pointed primarily at the east and west limbs, where models predicted the brightest intensity and where we had arranged for co-located observations with Hinode/EIS.

In the year leading up to the observation, AIR-Spec underwent significant upgrades to radically improve its sensitivity and image stability, and to correct two artifacts which appeared in the 2017 data. The IR camera manufacturer rebuilt the camera interface to remove light leaks, reducing the thermal background by a factor of 30 and removing its spatial structure. The upgrade resulted in more than five times higher SNR and significantly less error in the background subtraction. We added feedback to the image stabilization algorithm to reduce the root-mean-square (RMS) image motion by about a factor of six compared to the feedforward-only 2017 algorithm. We blocked stray reflections from the slit-jaw, which resulted in ghost images of the strong lines in the 2017 spectrum (Samra et al. 2019), and added mechanical constraints to the adjustable spectrometer mirrors to stop mirror vibration from distorting the lineshape. The improvements are evident in the example spectrum shown in Figure 2.

In 2019, AIR-Spec observed S XI 1.39 μm, Si X 1.43 μm, S XI 1.92 μm, and Fe IX 2.85 μm (Figure 2). The 1.39 μm S XI line was detected for the first time, and probable first detections were made of Si XI at 1.93 μm and Fe X at 1.95 μm (Samra et al. 2022a). The 3.93 μm Si IX line was not observed because the long-wavelength cutoff was reduced as part of the background-reduction effort, and the 3.03 μm Mg VIII line was not observed because the passband was tuned to observe the 1.39 μm line of S XI instead. The S XI

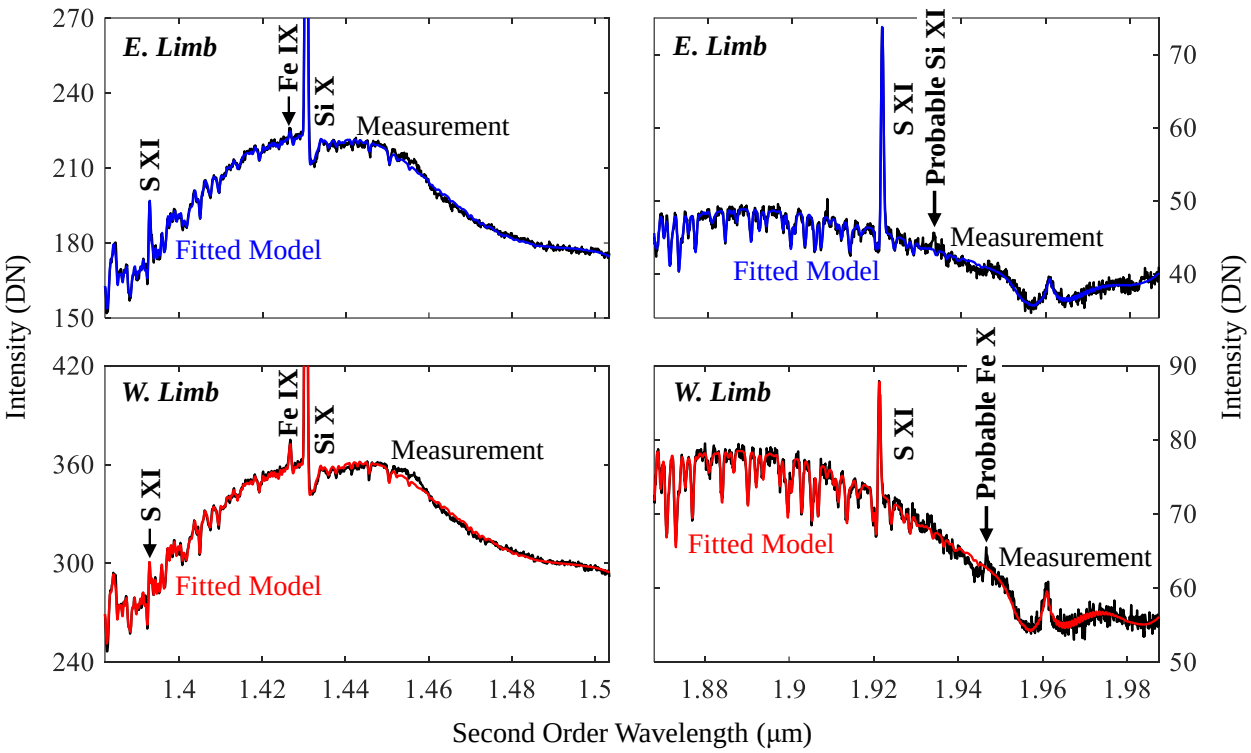

Figure 2. AIR-Spec measurement over 140 arcsec near the east and west limbs, average of 436 frames and 259 frames, respectively, at 0.25 second exposure time. An atmospheric model was used to extract accurate line intensities in the presence of significant telluric absorption, and fits are shown in blue and red.

line was chosen because it is half of a density-sensitive line pair and was unobserved at the time of the 2019 eclipse. Significant (5–10%) atmospheric absorption was measured near the emission lines, and atmospheric modeling was required to extract accurate line intensities (blue and red curves in Figure 2). The atmospheric structure helped us precisely calibrate the wavelength and instrument line shape and provided a check on the radiometric calibration, given some assumptions about the continuum brightness (Samra et al. 2022a). In the short-wavelength channel, it provided a way of separating the first and second-order continuum, as the absorption features only showed up in one order or the other.

Si X and S XI line intensities are plotted as a function of radial distance in panels 1, 3, and 4 of Figure 1. The improved sensitivity over the 2017 observations is evident in the much smaller error bars in the Si X fits. The measured and modeled intensity fall-off agree extremely well, implying that the relative contributions of radiative and collisional line excitation are well understood. Line ratios were used to measure the plane-of-sky (POS) temperature and density above the east and west limbs, the subject of a paper in progress. The measurements closely match the temperature and density estimated using measurements from AIA, EIS, and a ground-based polarization camera deployed by the NCAR High Altitude Observatory (HAO).

Broader Impacts: The 2019 re-flight provided projects for two REU interns. In 2018, Marissa Menzel assisted with the image stabilization system upgrade (Menzel et al. 2018). In 2019, Naylynn Tañón Reyes traveled to the eclipse operations base in Peru with the AIR-Spec team to do outreach in Spanish. She gave an AIR-Spec talk at Instituto Nacional de Investigación y Capacitación de Telecomunicaciones (INICTEL) on the campus of Universidad Nacional de Ingeniería and a tour of AIR-Spec to the local press and visiting professors (Tañón Reyes and Madsen 2020). After the eclipse, she completed a science project (Tañón

Reyes et al. 2020) using AIR-Spec data. The 2019 eclipse mission was featured in an NCAR press release and articles in *Forbes* and *El Comercio*.

Publications: A paper on the 2019 instrument and observations (Samra et al. 2022a) has been published and another paper on the coordinated density and temperature measurements is in progress.

2.3. MRI: Development of An Airborne Stabilized Platform for InfraRed Experiments (ASPIRE)

PI: Jenna Samra, Co-PIs: Edward DeLuca, Peter Cheimets, and Vanessa Marquez
Award #1919809, Amount: $697,975.00, Period of support: August 15, 2019–July 31, 2022

Intellectual Merit: ASPIRE, a versatile platform that can observe the Sun at a range of elevation angles and locations with a minimum of customization, is an extension of the successful AIR-Spec missions to the 2017 and 2019 total eclipses. It delivers a 20 cm beam stabilized to 6 arcsec RMS, providing four times the geometric area of the AIR-Spec feed and reducing the development time for new focal plane instruments.

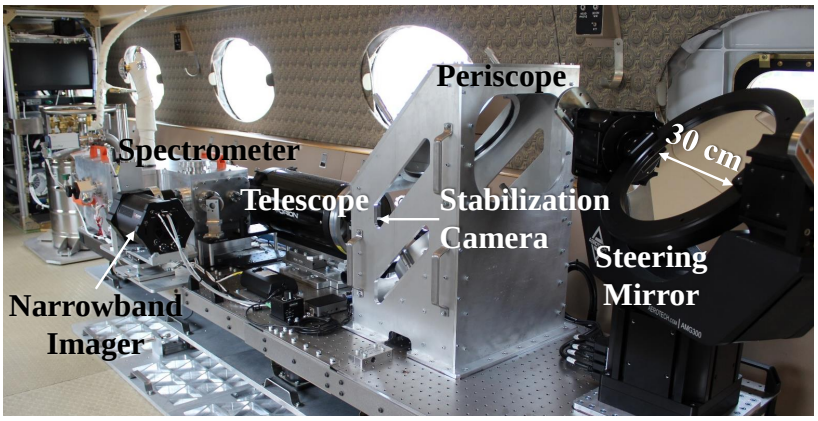

Figure 3. ASPIRE and commissioning focal plane instruments on the NSF/NCAR Gulfstream V.

Image stabilization is provided by a 30 cm gimballed steering mirror, gyroscope, and dedicated high-speed visible light camera. A periscope adapts the beam height to the focal plane instruments. During its commissioning flight, ASPIRE fed two first-light instruments: AIR-Spec with a larger telescope, and a new multi-thermal narrowband imager in Si X and S XI (Figure 3). In future flights, the image stabilization system (mirror, gyro, and camera) will be reflown with new focal plane instruments.

ASPIRE was originally scheduled to be commissioned during the December 14, 2020 total eclipse over South America, but the deployment was canceled due to the COVID-19 pandemic. NCAR was also forced to cancel the second commissioning flight, scheduled for the December 4, 2021 eclipse over Antarctica. Instead, ASPIRE was commissioned in December 2021 with three flights out of Broomfield, CO. Observations of the solar photosphere demonstrated the 6 arcsec RMS image stabilization performance, as shown in Figure 4. Analysis of solar and lunar observations will provide measurements of the spectral resolution, spatial resolution, and sensitivity of the two focal plane instruments.

Broader Impacts: Although the pandemic interrupted our plans for eclipse-related outreach, the creation of ASPIRE provided opportunities for public outreach presentations to the Amateur Telescope Makers of Boston and the Smithsonian's volunteer network. The commissioning flights were conducted by a team consisting entirely of early/mid-career scientists and engineers (Samra, Madsen, and Marquez), giving these individuals experience with campaign leadership and decision-making. ASPIRE turns the GV into a solar-pointed platform for general use by the solar and atmospheric communities.

Publications: A publication is in progress on the design and performance of the image stabilization system.

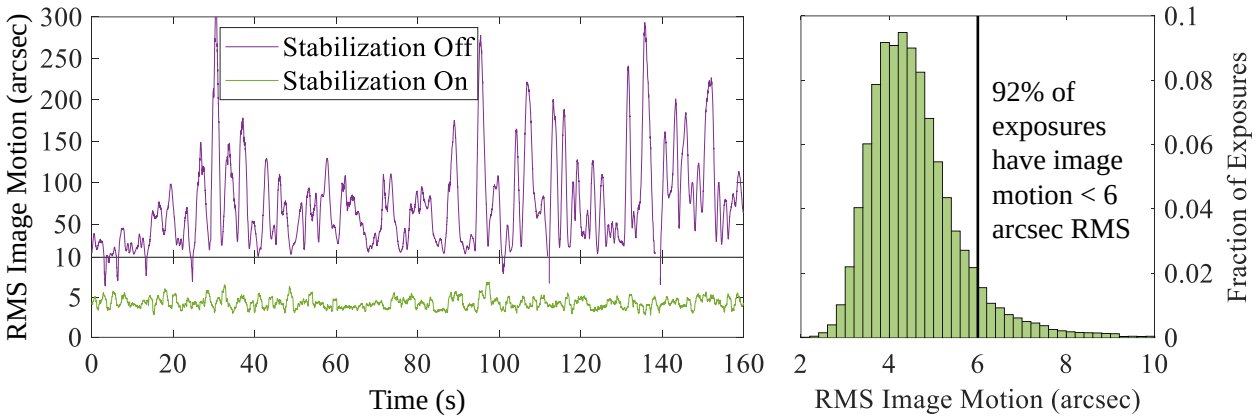

Figure 4. Image stabilization performance measured during one of the ASPIRE commissioning flights. Left: Comparison of 1-s RMS image motion over 160 seconds with and without image stabilization. Right: Histogram of 1-s RMS image motion over 30 minutes of flight in smooth air with image stabilization on.

2.4. MRI: Development of An Airborne Coronal Emission Surveyor (ACES)

PI: Jenna Samra, Co-PIs: Edward DeLuca, Peter Cheimets, and Vanessa Marquez
Award #2117582, Amount: $989,876.00, Period of support: September 1, 2021–August 31, 2024

Intellectual Merit: ACES is a new instrument that is being developed to explore the large-scale coronal IR emission spectrum. The program builds on our experience developing airborne IR instrumentation, including AIR-Spec and ASPIRE. Unlike AIR-Spec, a grating spectrometer that observed in a narrow passband, ACES is an imaging Fourier transform spectrometer (FTS) that will survey the entire 1–4 μm spectral range at high spectral resolution. If the current proposal is successful, ACES will be commissioned during the 2024 total solar eclipse from the NSF/NCAR GV with a solar feed provided by ASPIRE.

Over the past year, we have focused on selecting major system components (e.g. detector, mirror drive, corner cubes, beamsplitter, metrology system) and refining the system design based on the output of our models and conversations with FTS experts (especially James Hannigan of NCAR). Most significantly, we increased the camera frame rate in order to acquire ∼28 scans over the course of totality instead of just one. This required us to reduce the FOV to a 300 × 16 pixel "slot". In order to increase the SNR at the end of the slot furthest from the limb, we reduced the temperature of both the cryostat and the detector, decreased the focal length of the system, and increased the number of pixels binned. Instrument specifications are given in Table 1, with updates in bold, and the expected performance of the updated design is detailed in Section 3.3.

Broader Impacts: ACES adds a new early-career engineer to the team (led by Samra and Marquez) that built AIR-Spec and ASPIRE. Nora Casale is a junior engineer who will design the ACES software and electronics with oversight from senior SAO electrical engineers. In 2023, one of SAO's solar REU students will help us align and calibrate ACES in the laboratory. After

Scan length (OPD)	±2.5 cm
Sampling interval	316.5 nm
Scan time (2-sided)	**12.8 s**
Scan speed (OPD)	**3.9 mm s^{-1}**
Exposure time	**81 μs**
Frame rate	**12.3 kHz**
Aperture diameter	150 mm
Focal length	**370 mm**
Optical efficiency	0.4
Cryostat temperature	**150 K**
Detector temperature	**50 K**
Detector material	InSb
Pixel size	12 μm
Detector format	**300×16**
Binning	**3×16**

Table 1. ACES instrument specifications (updates in bold).

commissioning, ACES will be delivered to the NCAR High Altitude Observatory, where it will be available to the community for eclipse flights and/or ground-based coronagraphic observations.
Publications: The ACES MRI project has not yet resulted in any publications.

3. Proposed Investigation

We propose to commission ACES during the April 8, 2024 North American eclipse from GV HIAPER, with a solar feed provided by ASPIRE. A GV altitude of about 14 km will enable ACES to survey the near and mid-IR with minimal atmospheric interference. This section details the proposed investigation, including the science questions, measurement strategy, anticipated observations, and eclipse campaign.

3.1. Science Questions

During its commissioning flight, ACES will map emission line intensity as a function of radius along a coronal streamer. It is expected to observe neutral helium and up to 21 forbidden lines of ionized magnesium, aluminum, silicon, sulfur, argon, calcium, iron, and nickel (Table 2), and it may measure weaker lines of those and other ions. The eclipse mission addresses four main science questions:

Q1. What is the most information-rich set of coronal emission lines in the 1–4 μm range?

The infrared has strong tropospheric molecular absorption bands (Allen 1973). While theoretical coronal emission line intensities of abundant elements are well established (Judge 1998), to be able to use such lines for measurements of properties of magnetized coronal plasma, particularly from the new Daniel K. Inouye Solar Telescope (DKIST), accurate knowledge of the coronal emission and telluric absorption is required (e.g. Ali et al. 2022; Judge et al. 2002 for the case of Si IX 3934 nm in particular.) It is critical, especially for future studies of the coronal magnetic field, to identify the best possible coronal lines: they must be bright, form between electron temperatures of $10^{5.7}$ and $10^{6.5}$ K, extend as far as possible from the solar surface, and be free from damaging telluric extinction. In turn, the best lines are needed to fill in links from corona to heliosphere. For example, the formation of the He I 1083.3 nm triplet in the corona is complex and not well understood (Del Zanna et al. 2020). At low heights, it is expected to be comparable in strength to the nearby Fe XIII 1074.9 nm and 1081.1 nm lines (Kuhn et al. 1996, 2007). High-sensitivity ACES observations of a coronal streamer in He I and the two Fe XIII lines will help untangle the formation processes and dynamics inside interface outflow regions, and to help forecast the dynamics of eruptions and the wind through the low

λ (nm)	Ion	LogT (K)	FIP (eV)	SNR at 1.1 $R_\odot$ QS	AR
1014.3	Ar XIII*	6.45	15.76	0.0	18.6
1030.1	S XIII*	6.40	10.36	0.0	6.2
1074.9	Fe XIII	6.25	7.90	61.6	282.4
1080.1	Fe XIII	6.25	7.90	21.1	225.2
1083.3	He I	4.50	24.59	2.4	22.0
1252.4	S IX	6.05	10.36	16.2	10.9
1392.8	S XI	6.25	10.36	5.4	38.8
1430.5	Si X	6.15	8.15	66.4	141.7
1920.1	S XI	6.25	10.36	20.2	49.3
1935.0	Si XI*	6.20	8.15	1.7	18.0
1948.2	Fe X*	6.00	7.90	0.7	4.7
2045.0	Al IX*	6.05	5.99	3.0	4.8
2206.3	Fe XII*	6.20	7.90	8.3	24.8
2218.3	Fe IX*	5.90	7.90	1.6	12.3
2265.0	Ca XIII*	6.50	6.11	0.0	10.7
2430.7	Ni XI*	6.10	7.64	1.6	1.8
2482.6	Si VII*	5.80	8.15	1.2	9.1
2584.6	Si IX*	6.05	8.15	33.4	45.9
2856.3	Fe IX	5.90	7.90	3.1	10.9
3028.5	Mg VIII	5.90	7.65	3.1	18.9
3755.1	S IX*	6.05	10.36	2.2	2.6
3927.7	Si IX	6.05	8.15	42.1	26.0

Table 2. Strong lines in the 1–4 μm range. Density-sensitive line pairs and elements with high first ionization potential (FIP) are highlighted. Asterisks indicate lines that have not been observed (Del Zanna and DeLuca 2018). The last two columns give the predicted SNR in the peak intensity at 1.1 $R_\odot$ in the quiet Sun (QS) and an active region (AR).

corona (Kay and Gopalswamy 2017; Kilpua et al. 2019; Vourlidas et al. 2019).

The best lines must also be rich in diagnostic potential. Magnetic field measurements using the strongest pair of Fe XIII lines suffer from degeneracies due to the unpolarizable ground $J = 1 \rightarrow 0$ atomic level (Dima and Schad 2020). We have a strategy and code to remove the degeneracy, but only under the assumption that the magnetic signatures arise from a localized volume along the line of sight (Paraschiv and Judge 2022). A different approach to inferring magnetic information needs further scrutiny. Two ACES target lines, Si X 1430 nm and Mg VIII 3028 nm, form from less studied non-integer $J = 3/2 \rightarrow 1/2$ transitions. Schiffmann et al. (2021) showed that such non-integer J transitions can be coupled to Fe XIII to help ameliorate magnetic degeneracies, but multiple limitations in our understanding of Si X and Mg VIII exist. Good measurements from both ground and upper atmosphere of Mg VIII have been hard to achieve (Judge et al. 2001; Samra et al. 2022b), and its coronal height dependence has not been studied to our knowledge. Si X shows a very prominent intensity decrease with height, (see Figure 1, Figure 9 and Judge et al. 2001) and its profile is affected by potentially variable and blended telluric lines (e.g. Figure 10 of Ali et al. 2022). ACES will be able to remotely sense the solar height diagnostics at unprecedented heights of these very important ions for coronal magnetic diagnostics, while mitigating atmospheric influences that hinder their ground detection and interpretation.

A discrepancy exists between ground-based and high-altitude observations of prominent coronal lines. For example, in the case of Si IX 3934 nm, the upper atmosphere observations performed by Samra et al. (2022b) showed a good detection, while the scarce measurements from the ground (Judge 1998; Penn 2014) revealed barely detectable signals. This is unexpected, as such a striking difference did not manifest for other lines discussed above, but also because the atmospheric absorption at ground around 3934 nm is only significantly influenced by a sparsely spaced N_2O absorption band (Ali et al. 2022). Ground observations of such lines will become more common with the ramp-up of DKIST, but ACES is needed to clearly understand both the line formations and the influence of the atmosphere for ground or lower height observations in the near-IR.

Q2. How do plasma density and temperature vary with radial distance?

The so-called "middle corona" at $\sim 1.5 - 3$ $R_\odot$ is where many fundamental physical processes occur, resulting in the transition from the largely closed low corona to the open heliosphere. As this region of the corona is where CMEs and the solar wind are accelerated, measurements of its plasma parameters are crucial to being able to model and predict space weather. Identification of any ACES lines that are detectable out to 3 $R_\odot$ will help inform future IR instrument development.

Despite its importance, observations of the middle corona remain sparse and it is, consequently, poorly understood. Most EUV imaging instruments have a heliocentric FOV that extends no farther than ~ 1.7 $R_\odot$. These instruments are optimized for on-disk and low-corona observations, and the signal at the extremes of the FOV is often too low to be useful. Rare exceptions are the EUV analyses of Goryaev et al. (2014) and Seaton et al. (2021), both of which utilized instruments that were off-pointed from Sun center to image the middle corona. These studies are limited in their diagnostic capability, however, because they use broadband imaging instruments without spectral resolution. Spectroscopic measurements of the middle corona were routinely made by UVCS (Antonucci et al. 2005), but again these are limited in usefulness because the only emission lines with measurable signal beyond ~ 1.5 $R_\odot$were H I Ly α and O VI, whose emissivities are largely governed by photoexcitation and are thus poor diagnostics of the plasma. The result of this observational scarcity is that the radial variation of coronal temperature and density are unknown. In Fig. 5, duplicated from Del Zanna et al. (2018), we show the large range of values found in the literature for a streamer.

ACES will address this problem by probing the electron density (n_e), and electron and ion temperatures

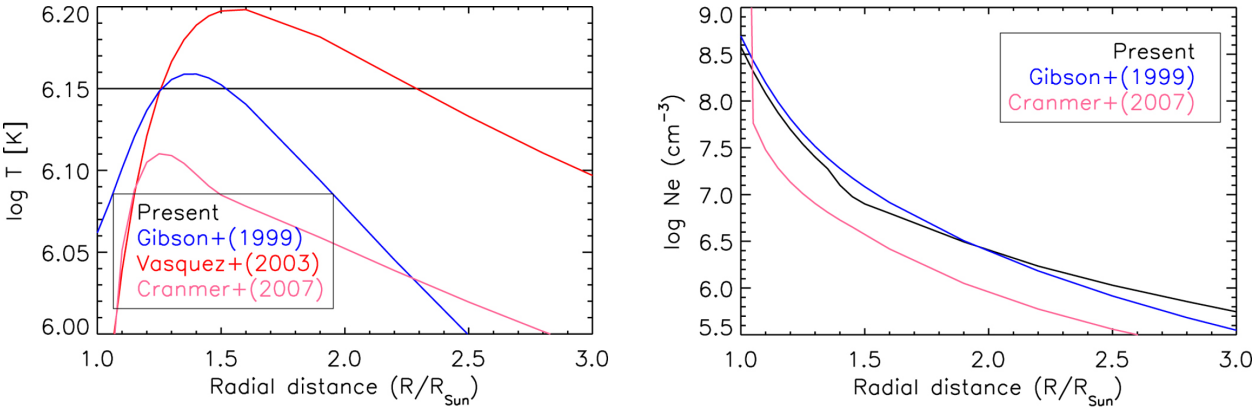

Figure 5. Electron density and temperature profiles in quiet Sun streamers. (Del Zanna et al. 2018)

(T_e and T_i) of a streamer as it extends into the middle corona. The richness of the spectrum over the ACES wavelength range allows for a measurement of multiple temperature and desity diagnostics (Table 2). Multiple line pairs with intensities sensitive to electron density (e.g. Mason 1991; Del Zanna and Mason 2018) lie in the ACES wavelength range. Four such pairs belonging to individual ions yield estimates of n_e without resorting to troublesome line ratios among multiple ions and elements (Judge 2020). These are highlighted in Table 2. The line pairs form in plasmas with a range of electron temperatures from $\log T = 5.90 - 6.25$ K, permitting testable density diagnostics for both quiescent and more active plasma. As shown in Fig. 9, the sensitivity of ACES will allow us to measure n_e to 1.65 $R_\odot$with moderate spatial binning, and even farther from the Sun with coarse binning. When combined with measurements of the K-continuum, ACES data will be used to probe density inhomogeneities as well as total and differential emission measures. Unlike extreme ultraviolet (EUV) diagnostics, IR line-ratio diagnostics can suffer uncertainties propagated from poorly understood local photoexcitation and temperature effects. ACES will help diagnose these by providing four distinct yet simultaneous line-pair measurements. We also point out that two of the line pairs used to determine n_e contain lines (Fe IX 2218.3 nm and Si IX 2584.6 nm) that have not been observed in the corona (Del Zanna and DeLuca 2018), expanding the discovery potential of the mission.

ACES will measure emission lines from several different ionization stages of Si, S, and Fe. Lines from a range of ions within the same element will be used to determine the T_e. This is only possible under the assumption of ionization balance, which breaks down in the corona as one measures farther from the solar surface (Boe et al. 2018). As the density decreases and the plasma becomes less collisional, ion fractionation "freezes in" and is no longer coupled to the local electron temperature, so we will determine T_e only out to this height. We will be able to determine the freeze-in height by comparing the line to continuum emission in a manner similar to that of Boe et al. (2018), giving an estimate of how this varies across the ions ACES will detect. At 2 $R_\odot$, ACES will measure the continuum with an error of only a few percent (Section 3.3).

ACES has sufficient spectral resolution (0.5 cm^{-1}, $\mathcal{R} \approx$ 20,000–5,000) to estimate *ion* temperatures T_i, by measuring widths of coronal lines, which is not affected by the freeze-in height the way T_e is. A large literature has studied multi-temperature and anisotropic distribution functions of coronal ions and electrons. Low in the corona, Tu et al. (1998) examined EUV data between 0.03 and 1.2 $R_\odot$ using the SUMER instrument on SoHO ($\mathcal{R} \approx 11,000 - 16000$, Wilhelm et al. 1997). Figures 2–4 of Tu et al. (1998) highlight problems in using data with modest resolutions. Still less convincing work has continued with the lower resolution EIS instrument on Hinode ($\mathcal{R} \approx 3000$, Zhu et al. 2021). Within the first scale height (50 Mm or 0.07 $R_\odot$) of the quiet corona, electron-ion energy equilibration times are about a minute. The switch from

collisional to collisionless electron-ion dynamics has never been fully explored; at 1.3 $R_\odot$ equilibration times are ≈ 1 hour, and many dynamical phenemona are documented at the coronal base between 1 minute and an hour (e.g. Cheung et al. 2022). Thus, the question remains an issue for probing roles of slower MHD versus fast collisionless processes in heating and accelerating the corona (e.g. Axford and McKenzie 2002). The UVCS instrument on SoHO measured profiles of H Lα and O VI lines at intermediate elongations of $2-4$ $R_\odot$ (Kohl et al. 1998), with evidence for anisotropic ion distribution functions in plasmas with far longer equilibration times. But these lines are not coronal, so that *there remains a gap in observations out to 2 $R_\odot$* in which reliable measurements are needed to examine the switch from fluid to kinetic physics controlling line profiles. *For the first time, ACES will provide independent information on T_e and T_i as a function of height in the corona out to 2 $R_\odot$.*

Q3. How does the ratio of radiative to collisional excitation vary with radius out to 2 $R_\odot$?

The visible and IR coronal emission lines arise from magnetic dipole transitions within the ground terms of np^m configurations of ions in the second and third rows of the periodic table ($n = 2, 3$ respectively, and $m = 3, 4, 5$). Observed atop the polarized K-corona's continuum emission, the lines are excited by collisions with local electrons (and protons), and by scattering of photospheric light. Collisional contributions dominate at higher densities low in the corona, acting to destroy the polarization naturally induced by scattering. The latter contains the imprint of magnetic field components owing to the geometry, as the coronal ions gyrate around field lines under the anisotropic photospheric irradiation. While beyond the scope of the present proposal, the future inference of magnetic fields using these lines will be fraught with challenges, requiring simultaneous solutions for plasma densities (discussed above) as well as magnetic parameters (Judge et al. 2021). In obtaining emission line intensities from 1 to 2 $R_\odot$, ACES will extend to magnetically-sensitive IR lines earlier visible measurements of the radial dependence of multiple line intensities. Under pure collisional conditions, these intensities fall off proportional to n_e^α where α lies between 1 and 2. Lines dominated by scattering system will result in a linear dependence upon electron density. When combined with density estimates below, ACES data will allow disentanglement of these processes, yielding a critical check on atomic models (Judge and Casini 2001) such as those used by the CHIANTI atomic database (Dere et al. 2019).

As shown in Figure 1, the 2017 and 2019 AIR-Spec observations produced preliminary results comparing radial radiance profiles of the strongest lines to theoretical profiles constructed using the collisional and photoexcitation models implemented by CHIANTI (Dere et al. 2019). ACES will expand on this work with its larger number and variety of lines, improved sensitivity, and ability to detect emission to 2 $R_\odot$.

Q4. How do elemental abundances vary with radius across the corona?

Decades of coronal observations have observed that under most quiescent conditions, elements of low FIP (< 10eV) are preferentially enhanced in the corona when compared to photospheric abundances while higher FIP elements remain the same or can become depleted. This is known as the FIP effect (Pottasch 1963). Low-FIP enhanced plasma is widely observed in active regions, the quiet Sun, and the slow-speed solar wind but is absent in coronal holes and fast-speed wind, making the FIP effect highly sensitive to the magnetic field topology and the thermal structure of the corona (Feldman et al. 1998; Baker et al. 2013).

Conversely, FIP-independent heavy elemental depleted helmet streamers have also been observed in the corona (Feldman et al. 1998; Raymond et al. 1997; Uzzo et al. 2003, 2004). The depleted streamers are thought to be connected with the development of gravitational settling in stable, long-lived coronal loops, where the heaviest elements (e.g. Fe) sink faster from the loop apex to its footpoints compared to lighter elements, resulting in mass-stratified plasma across the loop (Lenz et al. 1998). Alongside the FIP effect, these observations have suggested that gravitational settling may also play a role in governing the chemical makeup in coronal structures and the eventual plasma released as the solar wind.

Furthermore, while both processes are prominent in closed magnetic field structures, the FIP effect is thought to take place at the chromospheric-coronal boundary, while heavy ion dropouts become more pronounced above 1.3 $R_\odot$ (Feldman et al. 1998; Laming 2015). This suggests the existence of some radial dependence in chemical composition. Although the scientific literature contains a wealth of robust photospheric abundance measurements (e.g. Asplund et al. 2009, 2021; Scott et al. 2015a,b), it is currently not possible to determine the radial elemental composition within a single coronal structure to effectively constrain the two processes. The broad spectral sensitivity of ACES will shed light on this issue with unprecedented measurements of the radial FIP bias dependence from above the chromosphere to at least 1.5 $R_\odot$, enabling more detailed characterization of elemental composition throughout the corona necessary to identify the dominant fractionation mechanism.

ACES will allow for the measurement of absolute elemental abundances in the corona by measuring a variety of emission lines as well as the combined K- and F-continua. The measurement strategy follows that first described by Woolley and Allen (1948) and later adapted for observations of visible coronal emission during total solar eclipses (Mason 1975; Magnant-Crifo 1974; Habbal et al. 2021). By carefully comparing line and continuum intensities (the latter with the F-corona modeled and subtracted in outer regions), the atomic to hydrogen abundance can be estimated. Unlike Woolley and Allen (1948), we will be able take full advantage of the latest version of the CHIANTI atomic physics database (Dere et al. 2019). Combined with accurate models for the photospheric radiation, this allows us to avoid many of the ad-hoc assumptions imposed by Woolley and Allen (1948).

Through the broad wavelength range of ACES, we will determine simultaneous abundance measurements across seven elemental species: Ar, S, Fe, He, Si, Ca, and Mg, with a goal to measure abundances using spectroscopy higher than previously achieved. These sample a range of FIP values (Table 2) and masses. Given that FIP and mass have been demonstrated to be important determinants of coronal abundances, this permits us to further constrain those elemental fractionation processes occurring across coronal structures and their associated solar wind streams (e.g. Geiss et al. 1995; Duvernois and Thayer 1996; von Steiger et al. 2000; Laming 2015). ACES observations will uncover details of fractionation processes at the Sun and strengthen the link between coronal structures and their associated solar wind streams, addressing the causes of both the FIP effect and differential mass-stratification.

3.2. Measurement Strategy

The optical performance of ACES (Table 3) allows it to address the science questions in the previous section and meet the requirements in the Science Traceability Matrix with margin. The wavelength range captures the strong Fe XIII line pair at 1.07/1.08 μm and the Si IX line at 3.93 μm, as well as up to 18 other coronal forbidden lines and a He I triplet (Table 2). The coronal lines originate from a variety of ions and include many temperature and density-sensitive line pairs. The spectral plate scale provides more than three samples across the full width at half maximum (FWHM) of the narrowest emission line (Si IX 3.93 μm). The FOV is sufficient to image a streamer along one dimension from 1 to 3 $R_\odot$, and the spatial plate scale better than Nyquist samples the coronal scale height (0.07 $R_\odot$). Finally, the sensitivity is sufficient to detect the strongest lines at least 2 $R_\odot$ from disk center.

Wavelength range	1–4 μm
Spectral plate scale	0.2 cm^{-1}
Field of view	$2000'' \times 100''$
Spatial plate scale	$20'' \times 100''$ binned, $6.7'' \times 6.7''$ native
Sensitivity	SNR > 3 at 2 $R_\odot$

Table 3. ACES optical performance.

ACES consists of a condenser telescope and a Michelson interferometer (Figure 6). The condenser is a Gregorian telescope that provides a 5x compression of the beam. The beam exits the condenser to the side, allowing the central obscuration to be kept as small as possible, and enters the vacuum chamber that houses

the interferometer. The interferometer has a fixed mirror, a scanning mirror, and a beamsplitter to send light to each mirror and recombine the beams that return. After the two paths recombine, the light is focused onto the IR detector by an achromatic triplet made of CaF_2 and sapphire.

The moving mirror changes the optical path difference (OPD) between the two arms of the interferometer, modulating the fringe pattern at the detector. As the mirror is scanned from zero path difference (ZPD) to maximum path difference (MPD), the interferometer sweeps out a three-dimensional (spatial $\times$ spatial $\times$ OPD) image cube, with an interferogram at each spatial pixel. Fourier transforming each interferogram produces a spectrum, in wavenumber, at each pixel.

This measurement strategy allows ACES to observe a wide passband (1–4 μm) with relatively high spectral sampling (0.2 cm^{-1}) and a Nyquist-limited spectral resolution of about 0.5 cm^{-1}. The lens and 2D detector provide one-dimensional imaging along a "slot" FOV, of which the second dimension is truncated to allow for a higher frame rate. During each scan, the mirror moves slowly through a short range around ZPD in order to collect 2D (6 $R_\odot$ $\times$ 6 $R_\odot$) context images. Near ZPD, the detector well is close to full by design. Therefore, we expect these images to have high SNR despite the short exposure time.

As with the earlier AIR-Spec eclipse observations, the FOV rotation angle is set by the viewing geometry and the angle between Earth north and solar north. During the 2024 eclipse, the slot will be oriented about 41° from solar north. A streamer at the same angle will be chosen as the target. Figure 7 shows the full FOV and slot FOV superimposed on an image of the 2013 eclipse (© 2013 Constantinos Emmanoulidis, © 2014 Miloslav Druckmüller), approximately one full solar cycle before the 2024 eclipse.

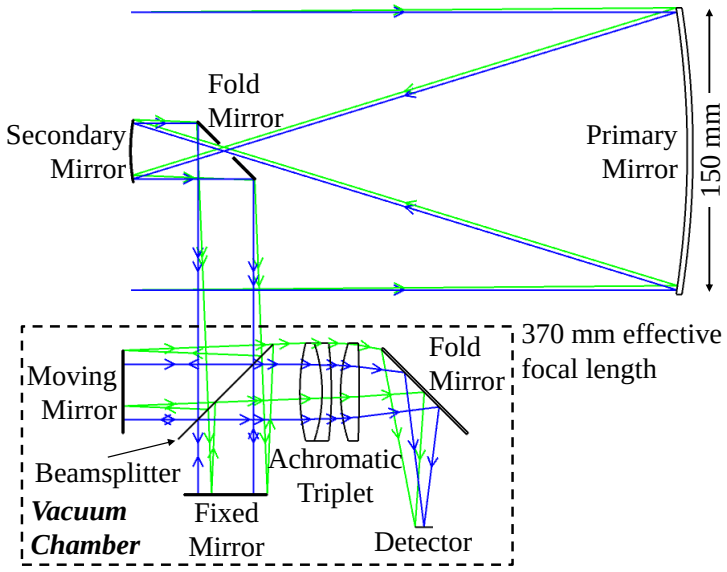

Figure 6. Ray trace of the ACES optical system.

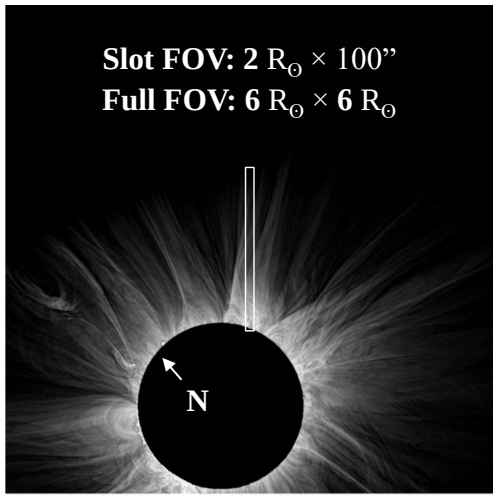

Figure 7. ACES FOV, full (context) and slot (spectra). The viewing geometry rotates the slot 41° relative to solar north.

3.3. Anticipated Observations

In order to assess the ACES sensitivity and spectral resolution, we simulated eclipse observations from the instrument. We used the quiet Sun model described by Del Zanna and DeLuca (2018) to simulate emission line intensity as a function of radius, a typical solar maximum coronal continuum profile (Golub and Pasachoff 2010, Figure 1.4), and a model of the atmospheric absorption spectrum from an altitude of 14.3 km (Lord 1992). The spectrum was formed at high resolution and inverse Fourier transformed to the OPD domain, and the resulting interferogram was truncated to the ACES scan length. The truncated

interferogram was summed with the expected thermal background and dark current, shot noise was added, and the noisy interferogram was quantized to the 14-bit depth of the camera ADC. Next, $16 \times 3 \times 28$ "measured" interferograms were averaged to model the effect of summing scans and binning pixels. Finally, the average interferogram was Fourier transformed to produce a "measured" spectrum. Figure 8 shows the measured ACES spectrum at 1 and 2 $R_\odot$.

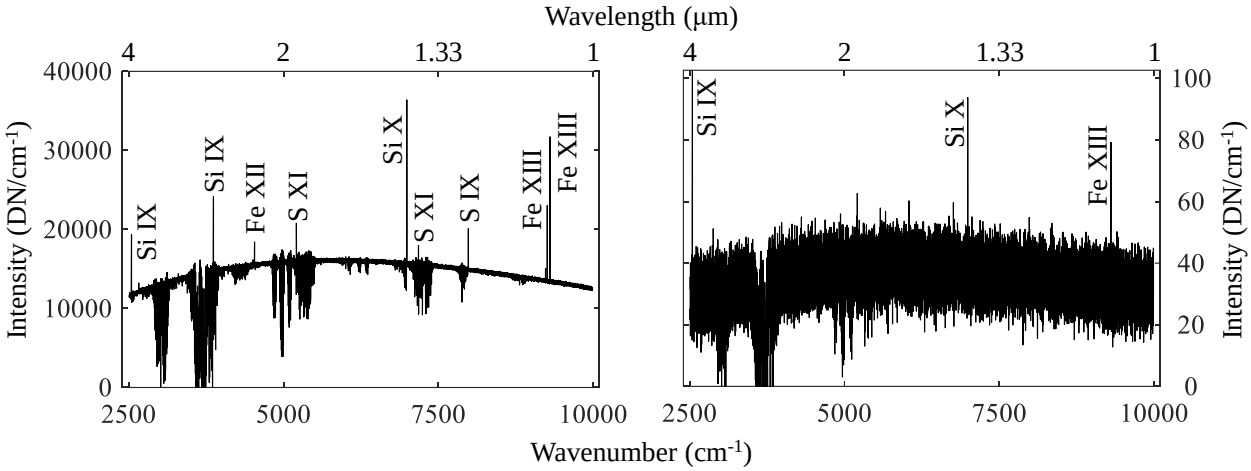

Figure 8. Expected ACES spectra at 1 $R_\odot$ (left) and 2 $R_\odot$ (right) from Sun center.

We used these simulated observations to evaluate the SNR in each line. The bar graph in Figure 9 shows the SNR in the line peak as a function of distance from Sun center. Each bar ends where SNR drops below three, providing a rough estimate of how far into the corona each line is detectable. At 1 $R_\odot$, 19 lines have SNR$>$ 3. Three lines, Fe XIII 1.07 μm, Si X 1.43 μm, and Si IX 3.93 μm, have SNR$>$ 3 as high as 2 $R_\odot$.

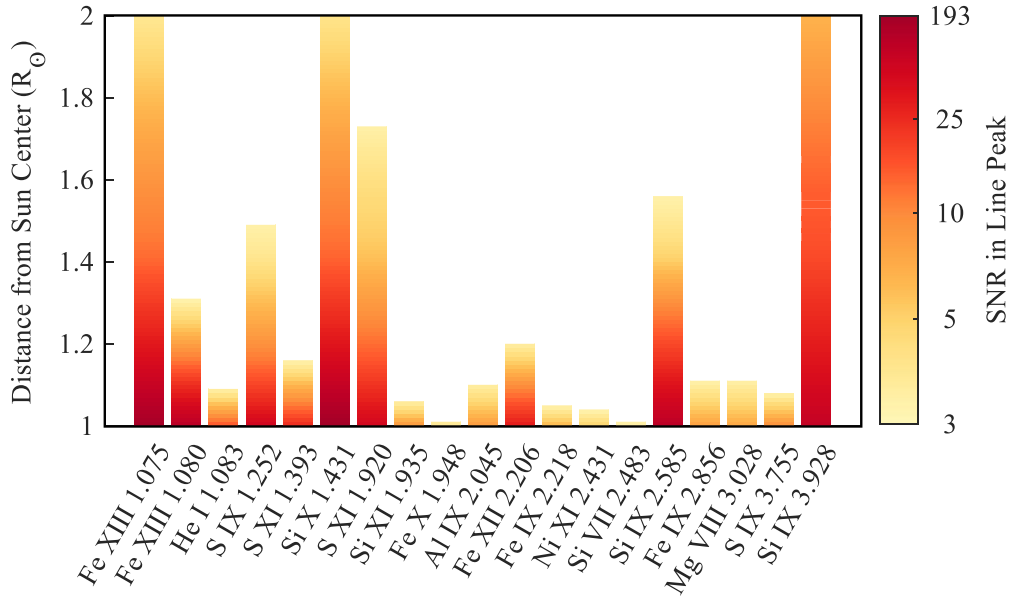

Figure 9. SNR as a function of distance from Sun center.

Gaussian fits to the noisy spectra provided an estimate of the measurement error in intensity, wavelength, and FWHM. Figure 10 shows fits to the three strongest lines at 1 and 2 $R_\odot$. At 2 $R_\odot$ the line peaks have SNR ranging from 3.4 to 5.8, resulting in errors in the fitted continuum and line intensities of only a few percent and errors in the fitted line wavelength and FWHM of well below 1%.

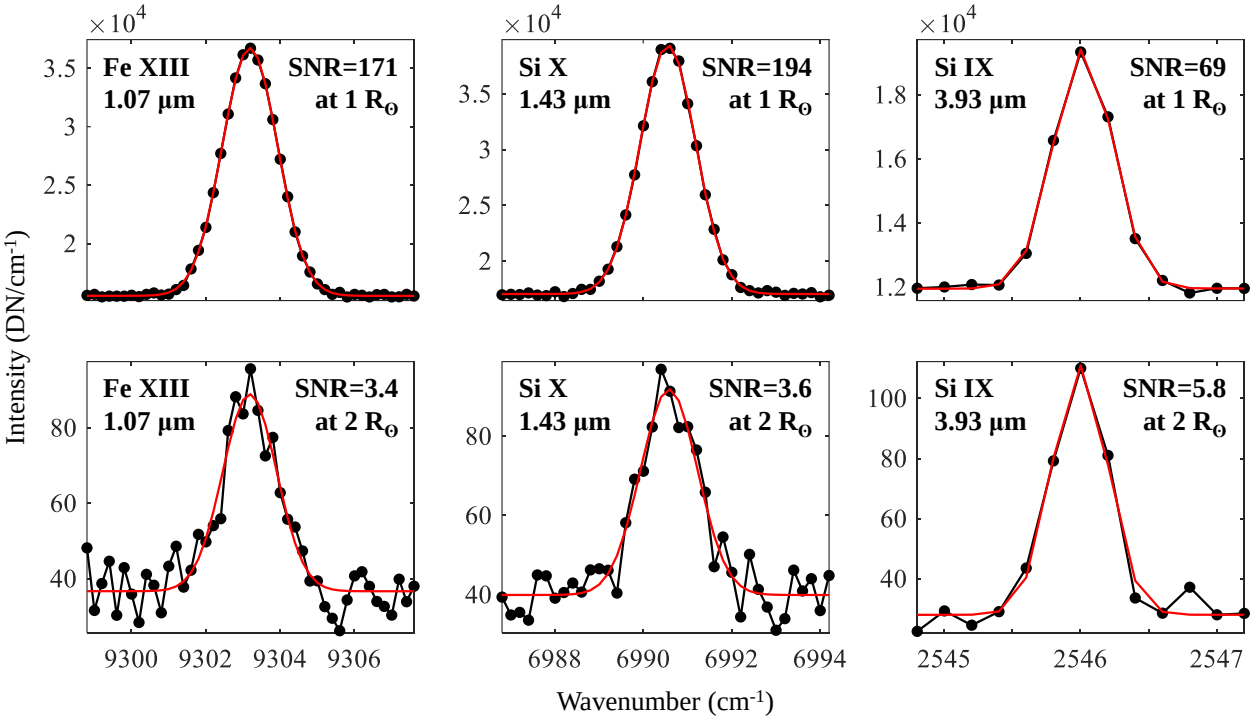

Figure 10. Fits to the strongest lines at 1 and 2 $R_\odot$. The simulated measurements are plotted in black and the line fits are shown in red.

Figures 8, 9, and 10 use line strengths from a quiet Sun model. We expect higher intensities during the 2024 eclipse, which will occur close to solar maximum. The last two columns in Table 2 compare the expected SNR at 1.1 $R_\odot$ in the quiet Sun (see also Figure 9) and an active region (Del Zanna and DeLuca 2018, Table 2). Table 2 includes three lines (Ar XIII 1014 nm, S XIII 1030 nm, and Ca XIII 2265 nm) that are missing from Figure 9 because they were not detectable even at 1 $R_\odot$ in the quiet Sun. They are expected to be measured with SNR $\approx$ 6–19 in an active region. The active region SNR is greater in the other lines as well, indicating that Figure 9 provides a conservative estimate of the maximum height for line detection.

Figure 11 shows the ACES measurement of Fe XIII 1.07 µm and Si IX 3.93 µm in the absence of noise. The natural line profile includes thermal broadening and a 25 km s^{-1} non-thermal e-folding linewidth. The constant ACES sampling of 0.2 cm^{-1} provides about 10 and 3.5 samples, respectively, across the FWHM of the Fe XIII and Si IX lines. The instrument line shape is a sinc function with width set by the mirror scan length. It has a negligible effect on the measured line shape, as shown in the figure. The spectral resolution is Nyquist-limited to about 0.5 cm^{-1} (2.5x the sampling), equivalent to $\mathcal{R} = 20,000$ at 10,000 cm^{-1} (1 µm) and $\mathcal{R} = 5,000$ at 2,500 cm^{-1} (4 µm).

3.4. Eclipse Campaign

The ACES team is well-versed in the unique challenges presented by airborne eclipse observations. PI Dr. Samra and Co-PI Dr. Madsen both took part in the successful AIR-Spec science campaigns that observed the

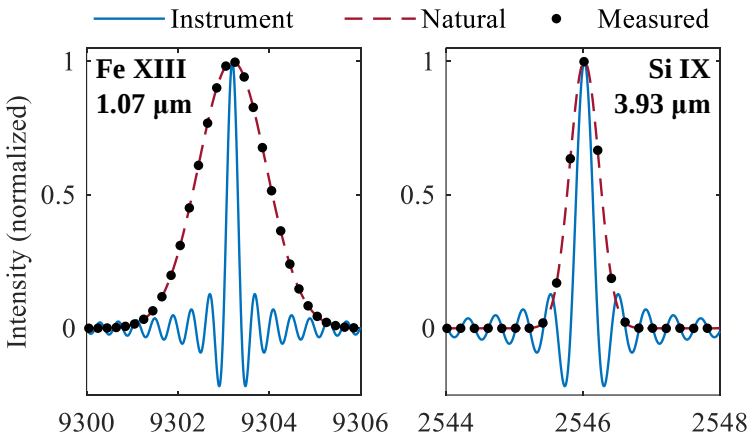

Figure 11. Instrument, natural, and measured line profiles.

2017 and 2019 total solar eclipses which also included successful coordination with external observatories. Drs. Samra and Madsen had also developed detailed observing plans for the eclipse flight of the 2021 ASPIRE mission which was ultimately canceled due to complications arising from the COVID-19 pandemic. As all of these missions took place aboard the NSF GV, the ACES team is familiar with its operation and capabilities. Given our prior success and familiarity with the aircraft, we propose a campaign similar to those carried out in our previous eclipse missions.

The preferred eclipse observation point is over the Pacific Ocean just off the coast of Mexico, with totality centered at 18:06 UTC. The preferred GV track is shown in blue in Figure 12 with the total eclipse path in red. We have chosen Brownsville, Texas as a tentative operating base given its proximity to the eclipse observation point, its location on the US-Mexico border (offering bilingual outreach opportunities), and its location near but not on the total eclipse path (reducing concerns of traffic or crowd-related delays on the day of the eclipse).

During the eclipse, ASPIRE and ACES will be mounted on the port side of the cabin toward the front of the plane. The optical bench and computer racks will be in the same positions they were in during the ASPIRE commissioning flights in 2021 (Figures 3 and 13). During the eclipse, ACES will observe out of a viewport mounted in the 18 inch overhead window at an elevation angle of about 70°.

Our observation will take place in three distinct phases: (1) a pre-flight preparatory phase, (2) a post-takeoff setup phase, and (3) a science phase during eclipse totality. The pre-flight phase begins approximately eight hours prior to takeoff when the instrument is first chilled by liquid nitrogen, a process that is familiar to the science team. The instrument's Dewar will be refilled every 10–30 minutes to account for evaporated losses. To prevent frosting of the optics when the instrument is chilled, a vacuum pump will evacuate the cryostat from several days before the observation until the GV is rolled out onto the ramp in preparation for takeoff. While on the ramp, a final round of chilling will be performed using a small handheld Dewar.

The setup phase begins when the GV reaches cruising altitude following takeoff. While in transit to the eclipse path, the optical bench will be unlocked and cranked into a predetermined position based on the calculated flight path. For particularly long flights, the instrument can be chilled again from a 25-liter Dewar installed in the GV cabin as was the case for the ASPIRE commissioning flights and the 2019 AIR-Spec flights. The GV will then enter a holding pattern one hour ahead of the total eclipse observation. The holding pattern serves two purposes: it allows us to absorb any schedule delays, and it gives us a number of opportunities to observe the Sun before it is fully eclipsed. One segment of the loops will be at a heading

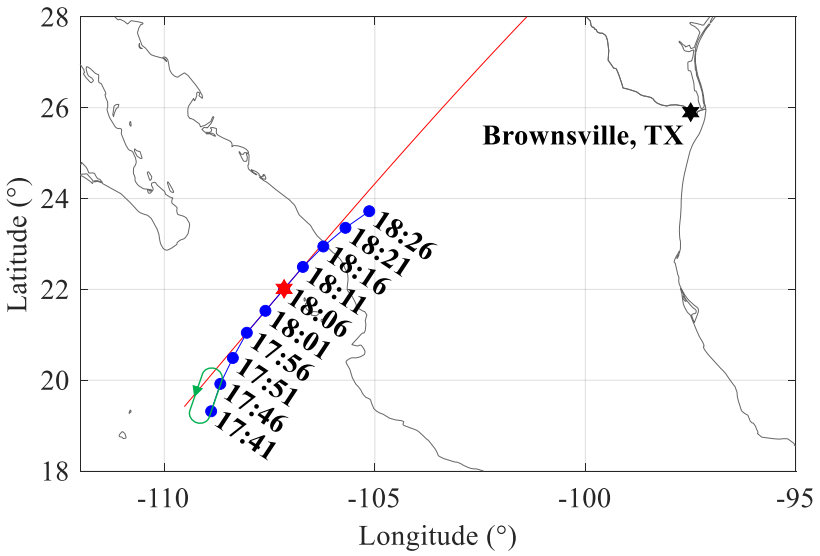

Figure 12. Preferred location for the 2024 eclipse observation. The middle of the observation occurs at 18:06 UTC. Brownsville, TX is the base of operations. The totality centerline is shown in red and the GV position is marked with blue circles. The first two points define the holding pattern (green ellipse).

such that the Sun is observable through the viewport, and we will use these passes to point the instrument at the Sun and take photospheric calibration data as well as darks. On the last pass, we will continue onto the eclipse centerline and wait for the Moon's shadow to overtake us. The GV will fly point-to-point until just before totality begins so that it does not drift too far from the eclipse centerline. Thereafter, it will hold a fixed heading to ensure that the planned solar azimuth angle is maintained in the presence of wind.

In the science phase, ACES will take data at a single pointing for the duration of the eclipse. We will select the brightest coronal feature, most likely a streamer or pseudostreamer, 2–3 days before the eclipse. The selection will be based on white-light eclipse forecast models that are regularly produced by the coronal modeling community (Downs et al. 2020, 2021; Pasachoff et al. 2021).

Coordinations with external observatories have proved fruitful in our previous eclipse missions and will be an important aspect of the ACES campaign. ACES team members have successfully coordinated with Hinode/EIS during the 2017 and 2019 eclipses, and we will build on that experience with ACES during the 2024 eclipse. Coordination with EIS will allow us to verify the physical diagnostics from the IR lines observed by ACES. The ACES team also initiated a collaboration with a National Solar Observatory (NSO) team that will coordinate ground-based 2024 eclipse observations with DKIST. One member of the NSO team, Dr. Kevin Reardon, is a collaborator on this proposal. Cryo-NIRSP observations of the same coronal structures a few hours after the eclipse will allow us to quantify the impact of the atmosphere on the DKIST line analysis (Ali et al. 2022). The DKIST/Cryo-NIRSP coordination will also permit us to study the continuum and dust corona via differential measurements. In addition to the compelling science pursued, this coordination will enhance the outreach and public dissemination components of both ACES and DKIST.

Given the rigid timing of the eclipse observation, the entire observing plan will be rehearsed several times in the weeks prior to the science flight. These will include simulations while the GV is grounded, test flights from NCAR RAF in Broomfield, CO, and two complete dry runs that follow the planned science flight path.

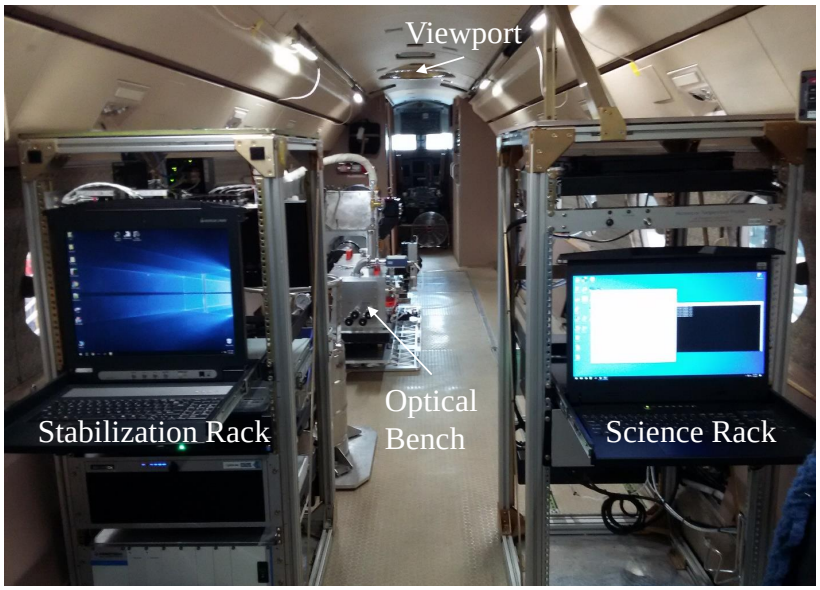

Figure 13. GV cabin layout for the 2024 eclipse.

4. Broader Impacts

New Research Infrastructure: After commissioning, ACES will be delivered to NCAR HAO, where it will be a valuable resource for the solar physics community. Due to its modular design, ACES can be repurposed for ground-based coronagraphic observations in addition to being flown in other eclipses. High-altitude studies with ACES may reveal new candidate emission lines for next-generation balloon- and space-borne instrumentation. Ground-based observations could be used to determine the practicality of observing particular lines in the presence of variable atmospheric transmission.

Student Education and Research Training: SAO has a strong Research Experience for Undergraduates (REU) program in solar physics, and five REU students have been involved throughout various stages in the development of AIR-Spec and ASPIRE. The ACES commissioning campaign will provide research training for at least two more students over the lifetime of the project. In summers 2024 and 2025, our students will analyze the recent eclipse observations and contribute to our papers in preparation. In addition, ACES will contribute to the training of at least one graduate student, Aatiya Ali (Georgia State University), who will be involved in the science and data analysis portions of the project.

Public Engagement with Science and Technology: Our previous eclipse missions have taught us that combining a total solar eclipse with the NSF GV is an excellent way to capture the public's attention. Based on our experience leading up to the 2017 North American eclipse, we expect significant interest from the press and general public in 2024. We have already begun discussions with Smithsonian Channel and a media group at Harvard about a possible video documentary on the ACES instrument build, test flights, and eclipse campaign. As these documentaries would be greatly enhanced by footage taken aboard the GV in flight, we are requesting permission from the NSF to fly media personnel on the GV on one or more of the ACES test flights if either of these collaborations comes to fruition.

The 2019 South Pacific eclipse gave us a unique opportunity to do solar physics outreach in Spanish while based in Lima, Peru, and we will build on that foundation in 2024 with outreach events in both the US and Mexico. In addition, the SAO team will reach out to their contacts at the University of Texas Rio

Grande Valley about the possibility of a bilingual outreach event at their Brownsville campus and other area schools.

Broadening STEM Participation of Underrepresented Groups: The ACES campaign team includes four women in early to mid-career STEM positions — Jenna Samra, Vanessa Marquez, Yeimy Rivera, and Daniela Lacatus — who are well-placed to attract young women to STEM fields. Ms. Marquez and Dr. Rivera are both members of the Hispanic/Latinx community, which is also underrepresented in STEM. The previous eclipse campaigns presented opportunities for outreach to underrepresented groups, including high-school girls at the Montrose School (an all-girls high school in Medfield, MA) and students from under-resourced communities at a meeting of Innovators for Purpose (a Cambridge-based organization that seeks to interest these students in science and technology). ACES will provide many more opportunities to engage in outreach with these and other groups.

5. Team Member Roles

The ACES science team includes the PI, two Co-PIs, and collaborators (many early and mid-career) from SAO, NCAR HAO, and NSO. Dr. Jenna Samra, the PI, will oversee the project, lead the flight campaign, and lead the low-level data processing of interferograms into spectra. She is currently leading the construction of the instrument on the MRI proposal. Dr. Yeimy Rivera, currently a post-doctoral researcher at Harvard, will be hired as an SAO scientist before the ACES science investigation begins. She will have a senior position on the project, contributing to the field campaign and leading the data analysis effort, especially the investigation of coronal abundances. Co-PI Dr. Chad Madsen (SAO) will lead the observation planning and EIS coordination efforts and assist in the data analysis effort. The final Co-PI, Dr. Paul Bryans of NCAR HAO, will lead the HAO collaboration. He will oversee the work of his early-career colleagues and provide guidance on their analysis efforts.

Our collaborators will contribute their expertise in coronal IR spectroscopy and coronal magnetometry. Dr. Alin Paraschiv (NCAR HAO) will use the ACES observations to understand the effects of Earth's atmosphere on the 1-4 μm coronal spectrum and to disentangle the atomic physics of emission lines that are prime candidates for coronal magnetometry. Dr. Daniela Lacatus (NCAR HAO) will lead the investigation of the transition from collisionally to radiatively-dominated excitation. Both Dr. Paraschiv and Dr. Lacatus will assist in supervising undergraduates and/or graduate students on the ACES analysis. Dr. Ryan French (NSO) and Dr. Kevin Reardon (NSO) will lead the coordination with DKIST. Dr. Philip Judge (HAO), an expert in atomic physics and coronal spectroscopy, will be a resource to the entire science team.

References

A. Ali, A. R. Paraschiv, K. Reardon, and P. Judge. A spectroscopic survey of infrared 1 - 4 μm spectra in regions of prominent solar coronal emission lines of fe XIII, si x, and si IX. *The Astrophysical Journal*, 932(1):22, jun 2022. doi: 10.3847/1538-4357/ac610a.

C. W. Allen. *Astrophysical Quantities*. Athlone Press, Univ. London, 1973.

E. Antonucci, L. Abbo, and M. A. Dodero. Slow wind and magnetic topology in the solar minimum corona in 1996-1997. *Astron. Astrophys.*, 435(2):699–711, May 2005. doi: 10.1051/0004-6361:20047126.

M. Asplund, N. Grevesse, A. J. Sauval, and P. Scott. The Chemical Composition of the Sun. *Annu. Rev. Astron. Astrophys.*, 47(1):481–522, Sept. 2009. doi: 10.1146/annurev.astro.46.060407.145222.

M. Asplund, A. M. Amarsi, and N. Grevesse. The chemical make-up of the Sun: A 2020 vision. *Astron. Astrophys.*, 653:A141, Sept. 2021. doi: 10.1051/0004-6361/202140445.

W. I. Axford and J. F. McKenzie. Coronal heating. *Advances in Space Research*, 30(3):505–505, Jan. 2002. doi: 10.1016/S0273-1177(02)00328-9.

D. Baker, D. H. Brooks, P. Démoulin, L. van Driel-Gesztelyi, L. M. Green, K. Steed, and J. Carlyle. Plasma Composition in a Sigmoidal Anemone Active Region. *Astrophys. J.*, 778(1):69, Nov. 2013. doi: 10.1088/0004-637X/778/1/69.

B. Boe, S. Habbal, M. Druckmüller, E. Landi, E. Kourkchi, A. Ding, P. Starha, and J. Hutton. The First Empirical Determination of the Fe^{10+} and Fe^{13+} Freeze-in Distances in the Solar Corona. *Astrophys. J.*, 859(2):155, June 2018. doi: 10.3847/1538-4357/aabfb7.

E. Cervantes Alcala, G. Guth, S. Fedeler, J. Samra, P. Cheimets, E. DeLuca, and L. Golub. Development of the User Interface for AIR-Spec. In *AGU Fall Meeting Abstracts*, pages SM51A–2458, Dec. 2016.

M. C. M. Cheung, J. Martínez-Sykora, P. Testa, B. De Pontieu, G. Chintzoglou, M. Rempel, V. Polito, G. S. Kerr, K. K. Reeves, L. Fletcher, M. Jin, D. Nóbrega-Siverio, S. Danilovic, P. Antolin, J. Allred, V. Hansteen, I. Ugarte-Urra, E. DeLuca, D. Longcope, S. Takasao, M. L. DeRosa, P. Boerner, S. Jaeggli, N. V. Nitta, A. Daw, M. Carlsson, L. Golub, and The. Probing the Physics of the Solar Atmosphere with the Multi-slit Solar Explorer (MUSE). II. Flares and Eruptions. *Astrophys. J.*, 926(1):53, Feb. 2022. doi: 10.3847/1538-4357/ac4223.

G. Del Zanna and E. E. DeLuca. Solar coronal lines in the visible and infrared: A rough guide. *The Astrophysical Journal*, 852(1):52, 2018. URL `https://doi.org/10.3847/1538-4357/aa9edf`.

G. Del Zanna and H. E. Mason. Solar UV and X-ray spectral diagnostics. *Living Reviews in Solar Physics*, 15(1):5, Aug. 2018. doi: 10.1007/s41116-018-0015-3.

G. Del Zanna, J. Raymond, V. Andretta, D. Telloni, and L. Golub. Predicting the COSIE-c signal from the outer corona up to 3 solar radii. *The Astrophysical Journal*, 865(2):132, oct 2018. doi: 10.3847/1538-4357/aadcf1. URL `https://doi.org/10.3847/1538-4357/aadcf1`.

G. Del Zanna, P. J. Storey, N. R. Badnell, and V. Andretta. Helium Line Emissivities in the Solar Corona. *Astrophys. J.*, 898(1):72, July 2020. doi: 10.3847/1538-4357/ab9d84.

K. P. Dere, G. Del Zanna, P. R. Young, E. Landi, and R. S. Sutherland. CHIANTI—An Atomic Database for Emission Lines. XV. Version 9, Improvements for the X-Ray Satellite Lines. *Astrophys. J. Supp. Series*, 241(2):22, Apr. 2019. doi: 10.3847/1538-4365/ab05cf.

G. I. Dima and T. A. Schad. Using Multi-line Spectropolarimetric Observations of Forbidden Emission Lines to Measure Single-point Coronal Magnetic Fields. *Astrophys. J.*, 889(2):109, Feb. 2020. doi: 10.3847/1538-4357/ab616f.

C. Downs, J. Linker, R. M. Caplan, R. Lionello, and P. Riley. Coronal Prediction for the December 14, 2020 Total Solar Eclipse. In *AGU Fall Meeting Abstracts*, volume 2020, pages SH030–0009, Dec. 2020.

C. Downs, J. Linker, P. Riley, R. Lionello, and R. Caplan. Remote Sensing and Global Coronal Models: Inputs, Constraints, and Lessons Learned. In *43rd COSPAR Scientific Assembly. Held 28 January - 4 February*, volume 43, page 1794, Jan. 2021.

M. A. Duvernois and M. R. Thayer. The Elemental Composition of the Galactic Cosmic-Ray Source: ULYSSES High-Energy Telescope Results. *Astrophys. J.*, 465:982, July 1996. doi: 10.1086/177483.

B. Edlén. Die Deutung der Emissionslinien im Spektrum der Sonnenkorona. Mit 6 Abbildungen. *Zeitschrift für Astrofysik*, 22:30, Jan. 1943.

S. Fedeler, J. Samra, and G. Guth. Development of Real-Time Image Stabilization for an Airborne Infrared Spectrometer. In *American Astronomical Society Meeting Abstracts #229*, volume 229 of *American Astronomical Society Meeting Abstracts*, page 437.02, Jan. 2017.

U. Feldman, U. Schühle, K. G. Widing, and J. M. Laming. Coronal Composition above the Solar Equator and the North Pole as Determined from Spectra Acquired by the SUMER Instrument on SOHO. *Astrophys. J.*, 505(2):999–1006, Oct. 1998. doi: 10.1086/306195.

J. Geiss, G. Gloeckler, R. von Steiger, H. Balsiger, L. A. Fisk, A. B. Galvin, F. M. Ipavich, S. Livi, J. F. McKenzie, K. W. Ogilvie, and B. Wilken. The Southern High-Speed Stream: Results from the SWICS Instrument on Ulysses. *Science*, 268(5213):1033–1036, May 1995. doi: 10.1126/science.7754380.

L. Golub and J. M. Pasachoff. *The solar corona*. Cambridge University Press, 2010.

F. Goryaev, V. Slemzin, L. Vainshtein, and D. R. Williams. Study of Extreme-ultraviolet Emission and Properties of a Coronal Streamer from PROBA2/SWAP, Hinode/EIS and Mauna Loa Mk4 Observations. *Astrophys. J.*, 781(2):100, Feb. 2014. doi: 10.1088/0004-637X/781/2/100.

S. R. Habbal, M. Druckmüller, N. Alzate, A. Ding, J. Johnson, P. Starha, J. Hoderova, B. Boe, S. Constantinou, and M. Arndt. Identifying the Coronal Source Regions of Solar Wind Streams from Total Solar Eclipse Observations and in situ Measurements Extending over a Solar Cycle. *Astrophys. J. Lett.*, 911(1): L4, Apr. 2021. doi: 10.3847/2041-8213/abe775.

P. Judge, B. Berkey, A. Boll, P. Bryans, J. Burkepile, P. Cheimets, E. DeLuca, G. de Toma, K. Gibson, L. Golub, J. Hannigan, C. Madsen, V. Marquez, A. Richards, J. Samra, S. Sewell, S. Tomczyk, and A. Vera. Solar Eclipse Observations from the Ground and Air from 0.31 to 5.5 Microns. *Solar Phys.*, 294 (11):166, Nov. 2019. doi: 10.1007/s11207-019-1550-3.

P. Judge, R. Casini, and A. R. Paraschiv. On Single-point Inversions of Magnetic Dipole Lines in the Corona. *Astrophys. J.*, 912(1):18, May 2021. doi: 10.3847/1538-4357/abebd8.

P. G. Judge. Spectral lines for polarization measurements of the coronal magnetic field. I. Theoretical intensities. *The Astrophysical Journal*, 500:1009–1022, 1998. URL https://doi.org/10.1086/305775.

P. G. Judge. Some thoughts on emission-line spectroscopy. *Monthly Notices of the Royal Astronomical Society*, 491(1):576–579, Jan. 2020. doi: 10.1093/mnras/stz3063.

P. G. Judge and R. Casini. A Synthesis Code for Forbidden Coronal Lines. In M. Sigwarth, editor, *Advanced Solar Polarimetry – Theory, Observation, and Instrumentation*, volume 236 of *Astronomical Society of the Pacific Conference Series*, page 503, Jan. 2001.

P. G. Judge, R. Casini, S. Tomczyk, D. P. Edwards, and E. Francis. Coronal Magnetometry: A Feasibility Study. Technical Report, PB2002-102493; NCAR/TN-466-STR, Jan. 2001.

P. G. Judge, S. Tomczyk, W. C. Livingston, C. U. Keller, and M. J. Penn. Spectroscopic Detection of the 3.934 Micron Line of Si IX in the Solar Corona. *ApJ*, 576:L157–L160, Sept. 2002.

C. Kay and N. Gopalswamy. Using the Coronal Evolution to Successfully Forward Model CMEs' In Situ Magnetic Profiles. *Journal of Geophysical Research (Space Physics)*, 122(12):11,810–11,834, Dec. 2017. doi: 10.1002/2017JA024541.

E. K. J. Kilpua, N. Lugaz, M. L. Mays, and M. Temmer. Forecasting the Structure and Orientation of Earth-bound Coronal Mass Ejections. *Space Weather*, 17(4):498–526, Apr. 2019. doi: 10.1029/2018SW001944.

J. L. Kohl, G. Noci, E. Antonucci, G. Tondello, M. C. E. Huber, S. R. Cranmer, L. Strachan, A. V. Panasyuk, L. D. Gardner, M. Romoli, S. Fineschi, D. Dobrzycka, J. C. Raymond, P. Nicolosi, O. H. W. Siegmund, D. Spadaro, C. Benna, A. Ciaravella, S. Giordano, S. R. Habbal, M. Karovska, X. Li, R. Martin, J. G. Michels, A. Modigliani, G. Naletto, R. H. O'Neal, C. Pernechele, G. Poletto, P. L. Smith, and R. M. Suleiman. UVCS/SOHO Empirical Determinations of Anisotropic Velocity Distributions in the Solar Corona. *Astrophys. J. Lett.*, 501(1):L127–L131, July 1998. doi: 10.1086/311434.

J. R. Kuhn, M. J. Penn, and I. Mann. The Near-Infrared Coronal Spectrum. *Astrophys. J. Lett.*, 456:L67, Jan. 1996. doi: 10.1086/309864.

J. R. Kuhn, J. Arnaud, S. Jaeggli, H. Lin, and E. Moise. Detection of an Extended Near-Sun Neutral Helium Cloud from Ground-based Infrared Coronagraph Spectropolarimetry. *Astrophys. J. Lett.*, 667(2):L203–L205, Oct. 2007. doi: 10.1086/522370.

J. M. Laming. The FIP and Inverse FIP Effects in Solar and Stellar Coronae. *Living Reviews in Solar Physics*, 12(1):2, Sept. 2015. doi: 10.1007/lrsp-2015-2.

D. D. Lenz, Y.-Q. Lou, and R. Rosner. Density Structure in a Multicomponent Coronal Loop. *Astrophys. J.*, 504(2):1020–1028, Sept. 1998. doi: 10.1086/306111.

S. D. Lord. A new software tool for computing Earth's atmospheric transmission of near- and far-infrared radiation. NASA Technical Memorandum 103957, Dec. 1992.

C. A. Madsen, J. E. Samra, G. Del Zanna, and E. E. DeLuca. Coronal Plasma Characterization via Coordinated Infrared and Extreme Ultraviolet Observations of a Total Solar Eclipse. *Astrophys. J.*, 880(2):102, Aug. 2019. doi: 10.3847/1538-4357/ab2b3c.

F. Magnant-Crifo. Absolute Abundances and Distribution of Material versus Density and Temperature in a Coronal Condensation. *Solar Phys.*, 39(1):141–151, Nov. 1974. doi: 10.1007/BF00154976.

H. E. Mason. The interpretation of the forbidden emission lines from a coronal condensation. *Monthly Notices of the Royal Astronomical Society*, 171:119–130, Apr. 1975. doi: 10.1093/mnras/171.1.119.

H. E. Mason. Density measurements in the corona. *Advances in Space Research*, 11(1):293–301, Jan. 1991. doi: 10.1016/0273-1177(91)90122-Z.

M. R. Menzel, J. Samra, V. Marquez, P. Cheimets, and E. DeLuca. Upgrading Stability of an Airborne Infrared Spectrometer (AIR-Spec) for Coronal Observations. In *AGU Fall Meeting Abstracts*, volume 2018, pages SH11C–2890, Dec. 2018.

A. R. Paraschiv and P. G. Judge. Efficient and Automated Inversions of Magnetically Sensitive Forbidden Coronal Lines: CLEDB - The Coronal Line Emission DataBase Magnetic Field Inversion Algorithm. *Solar Phys.*, 297(5):63, May 2022. doi: 10.1007/s11207-022-01996-5.

J. M. Pasachoff, C. Downs, J. Linker, R. Caplan, P. Riley, R. Lionello, A. Möller, V. Rušin, R. Vanur, and W. Carlos. Observational Validation of Predictions for the 2020 Eclipse Corona. In *American Astronomical Society Meeting Abstracts*, volume 53 of *American Astronomical Society Meeting Abstracts*, page 229.01, June 2021.

M. J. Penn. Infrared solar physics. *Living Reviews in Solar Physics*, 11(2):1, 2014. URL `https://doi.org/10.12942/lrsp-2014-2`.

S. R. Pottasch. The Lower Solar Corona: Interpretation of the Ultraviolet Spectrum. *Astrophys. J.*, 137:945, Apr. 1963. doi: 10.1086/147569.

J. C. Raymond, J. L. Kohl, G. Noci, E. Antonucci, G. Tondello, M. C. E. Huber, L. D. Gardner, P. Nicolosi, S. Fineschi, M. Romoli, D. Spadaro, O. H. W. Siegmund, C. Benna, A. Ciaravella, S. Cranmer, S. Giordano, M. Karovska, R. Martin, J. Michels, A. Modigliani, G. Naletto, A. Panasyuk, C. Pernechele, G. Poletto, P. L. Smith, R. M. Suleiman, and L. Strachan. Composition of Coronal Streamers from the SOHO Ultraviolet Coronagraph Spectrometer. *Solar Phys.*, 175(2):645–665, Oct. 1997. doi: 10.1023/A:1004948423169.

J. Samra, P. Cheimets, E. DeLuca, J. Galeros, T. Gauron, L. Golub, G. Guth, E. Hertz, P. Judge, S. Koutchmy, and V. Marquez. An airborne infrared spectrometer for solar eclipse observations. In C. J. Evans, L. Simard, and H. Takami, editors, *Ground-based and Airborne Instrumentation for Astronomy VI*, volume 9908 of *Proceedings of SPIE Astronomical Telescopes and Instrumentation*, page 99085U, 2016. URL `https://doi.org/10.1117/12.2232128`.

J. E. Samra, P. G. Judge, E. E. DeLuca, and J. W. Hannigan. Discovery of new coronal lines at 2.843 and 2.853 µm. *The Astrophysical Journal Letters*, 856(2):L29, 2018. URL `https://doi.org/10.3847/2041-8213/aab434`.

J. E. Samra, P. G. Judge, E. E. DeLuca, and J. W. Hannigan. Erratum: "Discovery of New Coronal Lines at 2.843 and 2.853 μm" (2018, ApJL, 856, l29). *The Astrophysical Journal*, 873(2):L25, Mar 2019. doi: 10.3847/2041-8213/ab0ae0. URL `https://doi.org/10.3847/2041-8213/ab0ae0`.

J. E. Samra, C. A. Madsen, P. Cheimets, E. E. DeLuca, L. Golub, V. Marquez, and N. T. Reyes. New observations of the IR emission corona from the 2019 july 2 eclipse flight of the airborne infrared spectrometer. *The Astrophysical Journal*, 933(1):82, jul 2022a. doi: 10.3847/1538-4357/ac6ce8. URL https://doi.org/10.3847/1538-4357/ac6ce8.

J. E. Samra, V. Marquez, P. Cheimets, E. E. DeLuca, L. Golub, J. W. Hannigan, C. A. Madsen, A. Vira, and A. Adams. The airborne infrared spectrometer: Development, characterization, and the 2017 august 21 eclipse observation. *The Astronomical Journal*, 164(2):39, jul 2022b. doi: 10.3847/1538-3881/ac7218. URL https://doi.org/10.3847/1538-3881/ac7218.

S. Schiffmann, T. Brage, P. G. Judge, A. R. Paraschiv, and K. Wang. Atomic Structure Calculations of Landé g Factors of Astrophysical Interest with Direct Applications for Solar Coronal Magnetometry. *Astrophys. J.*, 923(2):186, Dec. 2021. doi: 10.3847/1538-4357/ac2cca.

P. Scott, M. Asplund, N. Grevesse, M. Bergemann, and A. J. Sauval. The elemental composition of the Sun. II. The iron group elements Sc to Ni. *Astron. Astrophys.*, 573:A26, Jan. 2015a. doi: 10.1051/0004-6361/201424110.

P. Scott, N. Grevesse, M. Asplund, A. J. Sauval, K. Lind, Y. Takeda, R. Collet, R. Trampedach, and W. Hayek. The elemental composition of the Sun. I. The intermediate mass elements Na to Ca. *Astron. Astrophys.*, 573:A25, Jan. 2015b. doi: 10.1051/0004-6361/201424109.

D. B. Seaton, J. M. Hughes, S. K. Tadikonda, A. Caspi, C. E. DeForest, A. Krimchansky, N. E. Hurlburt, R. Seguin, and G. Slater. The Sun's dynamic extended corona observed in extreme ultraviolet. *Nature Astronomy*, 5:1029–1035, Aug. 2021. doi: 10.1038/s41550-021-01427-8.

N. Tañón Reyes and C. Madsen. Total Solar Eclipse Science and Outreach in Perú. In *American Astronomical Society Meeting Abstracts #235*, volume 235 of *American Astronomical Society Meeting Abstracts*, page 239.07, Jan. 2020.

N. Tañón Reyes, J. Samra, C. Madsen, and E. DeLuca. Eclipse Results from the Airborne Infrared Spectrometer (AIR-Spec) and the Extreme-ultraviolet Imaging Spectrometer (EIS). In *American Astronomical Society Meeting Abstracts #235*, volume 235 of *American Astronomical Society Meeting Abstracts*, page 210.09, Jan. 2020.

C. Y. Tu, E. Marsch, K. Wilhelm, and W. Curdt. Ion Temperatures in a Solar Polar Coronal Hole Observed by SUMER on SOHO. *Astrophys. J.*, 503(1):475–482, Aug. 1998. doi: 10.1086/305982.

M. Uzzo, Y. K. Ko, J. C. Raymond, P. Wurz, and F. M. Ipavich. Elemental Abundances for the 1996 Streamer Belt. *Astrophys. J.*, 585(2):1062–1072, Mar. 2003. doi: 10.1086/346132.

M. Uzzo, Y. K. Ko, and J. C. Raymond. Active Region Streamer Diagnostics 2001 September 14-16. *Astrophys. J.*, 603(2):760–775, Mar. 2004. doi: 10.1086/381525.

A. Vira. Alignment and Calibration of an Airborne Infrared Spectrometer. In *AGU Fall Meeting Abstracts*, volume 2017, pages SH13B–2481, Dec. 2017.

A. Vira, J. Samra, P. Cheimets, E. DeLuca, S. Fedeler, G. Guth, and V. Marquez. Image stabilization for Airborne Infrared Spectrometer. In M. Strojnik and M. S. Kirk, editors, *Infrared Remote Sensing and Instrumentation XXVI*, volume 10765 of *Proceedings of SPIE Optics and Photonics*, page 107650J, 2018. URL https://doi.org/10.1117/12.2319890.

R. von Steiger, N. A. Schwadron, L. A. Fisk, J. Geiss, G. Gloeckler, S. Hefti, B. Wilken, R. F. Wimmer-Schweingruber, and T. H. Zurbuchen. Composition of quasi-stationary solar wind flows from Ulysses/Solar Wind Ion Composition Spectrometer. *J. Geophys. Res.*, 105(A12):27217–27238, Dec. 2000. doi: 10.1029/1999JA000358.

A. Vourlidas, S. Patsourakos, and N. P. Savani. Predicting the geoeffective properties of coronal mass ejections: current status, open issues and path forward. *Philosophical Transactions of the Royal Society of London Series A*, 377(2148):20180096, July 2019. doi: 10.1098/rsta.2018.0096.

K. Wilhelm, P. Lemaire, W. Curdt, U. Schuhle, E. Marsch, A. I. Poland, S. D. Jordan, R. J. Thomas, D. M. Hassler, M. C. E. Huber, J. C. Vial, M. Kuhne, O. H. W. Siegmund, A. Gabriel, J. G. Timothy, M. Grewing, U. Feldman, J. Hollandt, and P. Brekke. First Results of the SUMER Telescope and Spectrometer on SOHO - I. Spectra and Spectroradiometry. *Solar Phys.*, 170(1):75–104, Jan. 1997. doi: 10.1023/A:1004923511980.

R. D. V. R. Woolley and C. W. Allen. The Coronal Emission Spectrum. *Monthly Notices of the Royal Astronomical Society*, 108:292, Jan. 1948. doi: 10.1093/mnras/108.3.292.

Y. Zhu, J. Szente, and E. Landi. Fe XII and Fe XIII Line Widths in the Polar Off-limb Solar Corona up to 1.5 $R_{\odot}$. *Astrophys. J.*, 913(1):74, May 2021. doi: 10.3847/1538-4357/abf1e3.